Permeation Dynamics of Small Molecules Through Silica Membranes: Molecular Dynamics Study

Hiromitsu Takaba, Koichi Mizukami, Momoji Kubo, Adil Fahmi, and Akira Miyamoto
Dept. of Materials Chemistry, Tohoku University, Sendai 980-8579, Japan

The permeation of He, CO_2, and N_2 through a thin silica membrane was investigated using molecular dynamics. The permeance of He follows Knudsen flow. The permeation of CO_2 is higher than the estimated value from Knudsen theory. Inside the pore, CO_2 tends to be parallel to the pore wall. This orientation is suitable for diffusion. In contrast, N_2 shows lower permeance compared to the value from Knudsen theory. The molecules present perpendicular orientations inside the pore wall, which reduces their diffusion. In mixed CO_2/N_2 gas simulation, the selective permeation of CO_2 relative to N_2 was observed.

Introduction

Much attention has been given to the gas separation using porous inorganic membranes because of their high permeabilities relative to dense inorganic membranes and their thermal and chemical stabilities relative to organic membranes (Hsieh, 1996). For the separation of small gas molecules using inorganic membranes, a thin membrane with very sharp pore distribution and without pinholes is often required. Since silica membranes can satisfy this requirement, much effort has been devoted to the preparation of microporous silica membranes.

Certain gases such as hydrogen (Gavalas et al., 1989; Jiang et al., 1995) and carbon dioxide (Li and Hwang, 1992; Sea et al., in press) selectively permeate through silica membranes. Their transport properties depend on the texture of the membrane. The pore size and distribution and the interaction between the permeating molecules and the membrane wall are of fundamental importance in determining the transport mechanism. It is therefore very important to have some guidelines from theoretical models that can provide an atomistic description of the permeation process and can help in developing membranes appropriate for a specific gas separation.

Some theoretical studies have been done. Fain and Roettger (1993) and Shelekhin et al. (1995) have shown the relationship between the separation factor and the pore size for several transport mechanisms. Molecular dynamics (MD) methods allow the description of the dynamics behavior of the permeated molecules through the membrane. Cracknell et al. (1995) and Furukawa et al. (1996) investigated the permeation flux on a slitlike simple model membrane using nonequilibrium MD. We applied MD to investigate the effect of the membrane affinity on the permeation process (Takaba et al., 1996) and the permeation of butane isomers through a zeolite membrane (Takaba et al., 1997). So far, however, no work has been reported on the transport mechanism through a silica membrane.

In the present work we report MD simulations of He, CO_2, and N_2 permeation on a silica membrane and describe their transport mechanisms at the atomistic level. Helium is often used as a probe gas in experiments to characterize the membrane performance for permeation. Furthermore, the N_2/CO_2 mixed system is much more attractive because of the importance of the separation technology of CO_2 from the exhaust gas.

Fundamentals of Gas Transport on Inorganic Membranes

Four transport mechanisms through inorganic membranes are often discussed: Knudsen diffusion, surface diffusion, capillary condensation, and molecular sieving mechanisms (Koros and Fleming, 1993; Saracco and Specchia, 1994). The Knudsen diffusion mechanism gives relative permeation rates that are equal to the inverse square root ratio of the molecular weights of the gases. This mechanism can be applied when the mean free path of the molecules is greater than the pore diameter, and collisions of the molecules with the pore walls occur more frequently than collisions between diffusing

Correspondence concerning this article should be addressed to A. Miyamoto.

molecules. By decreasing the pore size and increasing the interaction between the molecules and the membrane wall, other transport mechanisms appear. For strong adsorption, the molecules adsorb and diffuse on the pore wall, making the transport a surface diffusion. Besides, with high pore occupancy, accumulation of the molecules in the pore leads to the capillary condensation mechanism. On the other hand, for a mixed gas, only species that have a diameter smaller than that of the pore will diffuse, and the membrane shows molecular sieving. Bakker et al. (1996) used the configurational diffusion concept to interpret the transport through a zeolite membrane. The basic idea is that molecules move from one adsorption site to another within the pore. By increasing the temperature, the kinetic energy of the molecules increases, whereas the interaction with the adsorption sites remains rather constant.

Experimentally, it is difficult to determine the transport mechanism because both physical and chemical conditions affect diffusion behavior. Besides, for microporous membranes (amorphous silica and zeolites), physical (pore size and membrane structure) and chemical (adsorption sites) properties are difficult to analyze. Therefore theoretical methods are a useful tool for investigating transport mechanisms.

Method of Calculation

NVT ensemble (constant volume, number of particle, and temperature) MD simulations were performed based on the MXDORTO program (Kawamura, 1992). In this program we modified the control of the temperature and introduced an intramolecular potential to describe the bonding within a gas molecule (N_2 and CO_2). In the simulation of gas permeation it is important to keep the temperature of all atoms at a desired level. Therefore the temperatures of the solid and gas regions were controlled separately in order to keep these temperatures at desired levels during the simulation. The temperature was controlled by means of scaling atomic velocities under three-dimensional periodic boundary conditions. The validity of this method was demonstrated in our previous works (Takaba et al., 1996; Mizukami et al., 1997). The motion of the atom i on the potential energy surface of the system with energy $E(R)$ is described by Newton's equation of motion as follows:

$$-\frac{dE}{dR} = m\frac{d^2R}{dt^2}. \tag{1}$$

The MD code derives the solution to Eq. 1, using an empirical fit to the potential energy surface for the motion of all atoms in the system. This equation is numerically integrated by the Verlet algorithm, using small (1.0×10^{-15} s) time steps in producing a trajectory of the system. The Ewald method was used to calculate the electrostatic interactions.

The empirical fit to the potential energy was performed using the following expression for any atoms i and j:

$$E(R) = \sum_i \sum_{j>i} \frac{Z_i Z_j e^2}{r_{ij}} \tag{2a}$$

$$+ \sum_i \sum_{j>i} f_o(b_i + b_j)\exp\left[(a_i + a_j - r_{ij})/(b_i + b_j)\right] \tag{2b}$$

$$+ \sum_\beta D_b\left\{1 - \exp[-a(\beta - \beta_0)]^2\right\} \tag{2c}$$

$$+ \sum_\theta h_\theta(\theta - \theta_0)^2 \tag{2d}$$

$$+ \sum_i \sum_{j>i} \left[\frac{(A_i A_j)^{1/2}}{r_{ij}^{12}} - \frac{(B_i B_j)^{1/2}}{r_{ij}^{6}}\right]. \tag{2e}$$

These potentials correspond, respectively, to Eq. 2a Coulomb; Eq. 2b exchange-repulsion; Eq. 2c angle bending; Eq. 2d bond stretching; and Eq. 2e Lennard-Jones potentials. The interaction between membrane atoms (Si, O, and H), which was used to make the amorphous silica structure, was described by potentials (Eqs. 2a, 2b, 2c). The angle bending potential (Eq. 2b) was applied for the formation of Si–O–H. The interaction between nonbonded species—gas molecule–gas molecule and membrane–gas molecule—was presented by potential (Eqs. 2a and 2e). The intramolecular potential for gas molecules (N_2 and CO_2) was described by potential (Eqs. 2c and 2d). Z_i is the atomic charge, e is the elementary electric charge, r_{ij} is the interatomic distance, and f_o ($=6.9511\times10^{-11}$ N) is a constant for unit adaptations. The parameters a_i and b_i represent the size and the stiffness of atoms, respectively; A_i and B_i represent Lennard-Jones energy and length, respectively; β and θ are the bond stretching and the angle bending, respectively; and D_b, α, h_θ, θ_0, and β_0 are constants. All the potential parameters, which were established by fitting MD results to experimental thermodynamic properties or quantum chemistry results, are listed in Table 1.

The dynamic features of the system are observed by using the real-time solid modeling visualization program RYUGA (Miura et al., 1995).

Model for the Silica Membrane

Figure 1 shows our model for the silica membrane. The unit cell has the following dimensions: $a = 31.2487$ Å, $b = 32.3326$ Å, and $c = 80.0$ Å. This model is built using MD and referring to a method reported by Feuston and Garofalini (1989). To make a solid amorphous silica, the bulk of cristobalite is melted at 4,000 K. Then it is quenched at a rate of 2.5 K per fs from 4,000 K to 300 K. The membrane surface is created by removing the periodicity in the z-direction, and the system becomes periodic in the x- and y-directions. By removing some atoms from the obtained solid, we created a micropore. Next, we relaxed the surface at 300 K for 10 ps to obtain a more stable system. This surface contains some unsaturated oxygen and silicon atoms that have less coordination compared to bulk atoms. In operating conditions, silica membranes are always hydroxylated. Therefore we added hydrogen atoms and hydroxyl groups to unsaturated surface O and Si atoms, respectively. This system is again relaxed at 300 K for 10 ps. The equilibrium structure presents an effective pore diameter of equivalent capillary of 8 Å and a thickness of 14 Å. The pore is not perfectly circular, and runs in the direction from the gas region to the vacuum region. The pore surface is rather rugged, as shown in Figure 1. In the permeation simulations, only the gas molecules are allowed to move, and the positions of membrane atoms are fixed.

Table 1. Potential Parameters Used in this Study

Atom	Ref.	Mass/ mol^{-1}	Z	a/Å	b/Å
O (Silica)	1	16.00	−1.20	2.0474	0.17566
Si	1	28.08	+2.40	0.8688	0.03285
H	2	1.00	+0.60	—	—
N	3	14.00	0.0	—	—
He	4	4.00	0.0	—	—
O (Carbon dioxide)	5	12.01	−0.298	—	—
C	5	14.01	+0.596	—	—
Bond Stretching		D_b/kcal·mol^{-1}	β/Å^{-1}	β_0/Å^{-1}	
O–C	6	145.0	2.060	1.23	
N–N	6	226.8	2.6829	1.09758	
Angle		h_θ/kcal·mol^{-1}·rad^{-1}		θ_0/degree	
Si–O–H	2	118.0		33.1	
O–C–O	6	145.0		180.0	
Lennard-Jones		A_{ii}/kcal·mol^{-1}·Å^{12}		B_{ii}/kcal·mol^{-1}·Å^6	
O (Silica)	2	272,894.7846		498.8788	
	1	0.0*		4951.94*	
Si	2	3,149,175.0000		710.0000	
	1	0.0*		537.31*	
H	2	0.00001		0.0000	
N	6	512,394.114		389.61545	
He	4	741.741435		2.6914715	
O (Carbon dioxide)	5	1,484,322.789		990.1850584	
C	5	200,709.8836		498.87880	

*Note: Parameters of *Thuneyuki* potential for describing the interaction between Si and O atoms. These are only used for the simulation of making the amorphous silica structure.

(1) Tsuneyuki et al., 1988; (2) Dauber-Osguthorpe et al., 1933; (3) Cheung and Powles, 1975; (4) Reid et al., 1987; (5) Murthy et al., 1981; (6) bond-stretching parameters derived from diatomic bond length and stretching data are from Herzberg (1950) and from the *CRC Handbook of Chemistry and Physics*, 54th ed., 1973–1974.

In order to examine the validity of our model, radial distribution functions (RDF), which describe the distribution of atom–atom distances, and the concentration of silanol groups (Si–OH) on the surface are compared to experimental data. The first three peaks in the RDFs appear at 1.60 Å, 2.71 Å, and 3.29 Å, which correspond to Si–O, O–O, and Si–Si distances, respectively. These values are in good agreement with those obtained from both X-ray diffraction and neutron scattering results (Narten et al., 1972; Misawa et al., 1980; Sinclair and Wright, 1974): 1.60–1.62 Å, 2.62–2.65 Å, and 3.11–3.13 Å. However, the concentration of hydroxyls at the surface is approximately 3×10^{-2} mol/Å^2, which is smaller than the experimental value of 4×10^{-2}–6×10^{-2} mol/Å^2 (Iler, 1979). Therefore the experimental membrane presents a defected structure that can accommodate a larger number of hydroxyls.

To describe the permeation mechanism we compare our MD results with the Knudsen flow theory. The system follows the Knudsen diffusion mechanism when the following condition is satisfied (Hwang and Kammermeyer, 1975):

$$r/\lambda < 1, \tag{3}$$

where r is the pore radius and λ is the mean free path of the molecule. We performed our calculations in similar conditions. For short capillaries as in our membrane model, the

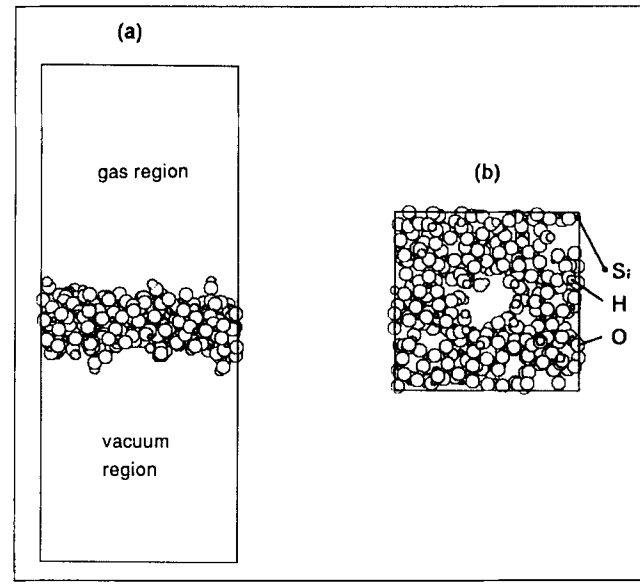

Figure 1. Model for the silica membrane: (a) side view; (b) top view.

permeability in the Knudsen or transition range is given by (Carmine, 1956):

$$q = \frac{4\delta_0}{3k_1}\frac{r}{2L}\nu(1+k_2 r/2\lambda)\frac{\Delta p}{p_1}, \tag{4}$$

where L is the length of porous sample in direction of flow, which is 14 Å in our model, Δp is the pressure difference between the gas and vacuum regions, ν is the mean thermal molecular velocity, p_1 is the pressure of the gas region; k_1 is the shape factor given by

$$k_1 = 1 + \frac{16}{3}\frac{r}{2L}, \tag{5}$$

and k_2 as well as k_1 is a function of $r/2L$. Knudsen flow applies strictly to $r/\lambda = 0$. The correction term related to the deviation from such an ideal condition is k_2. For capillaries where L is less than $8r$, k_2 becomes 0 (Hiby and Pahl, 1952). Assuming a perfect gas and $k_2 = 0$, Eq. 4 becomes

$$q = \frac{4\delta_0}{3k_1}\frac{r}{2L}\sqrt{\frac{8RT}{\pi M}}(1+k_2 r/2\lambda)\frac{n_1(t)V_2 - n_2(t)V_1}{n_1 V_2}, \tag{6}$$

where M is the molecular weight, R is the perfect-gas constant, T is the temperature, n_1 and n_2 are the number of molecules in the gas and vacuum regions, respectively, at time t of the simulation, and the total number of molecules is 64. V_1 (30, 310 Å^3) and V_2 (30, 325 Å^3) are the gas and vacuum region volumes. The permeance of Knudsen flow is calculated from the integration of Eq. 5 with respect to time t.

Results and Discussion

Helium permeation

To obtain the correct configuration for the initial state of the helium gas, we relaxed the molecules, but not the mem-

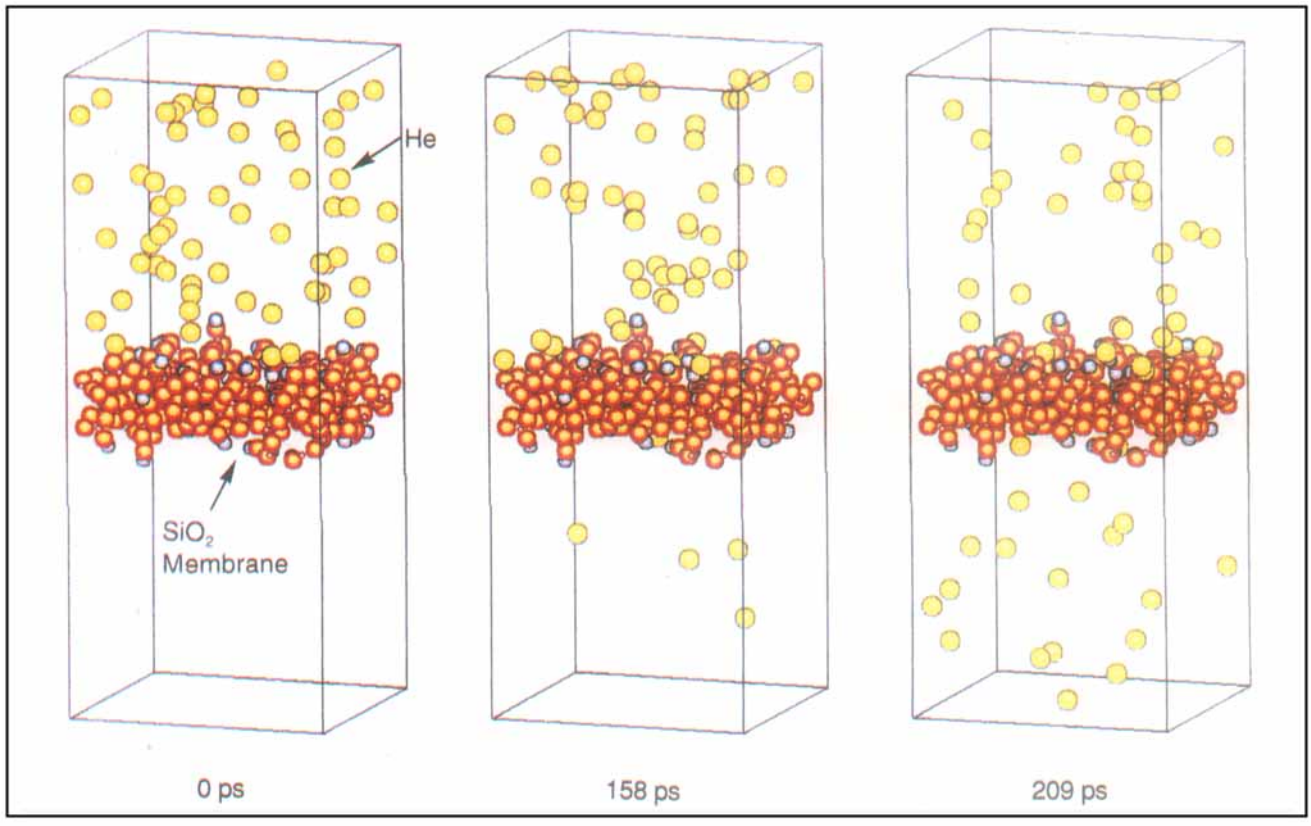

Figure 2. Permeation of the He single gas at 500 K.

brane, within a volume corresponding to the gas region volume. Next, the configuration of minimum energy was put in the gas region over the membrane. In this way we avoided the rapid increase in temperature that can be caused by intermolecular repulsions. The permeation simulations show that helium atoms diffuse randomly and permeate through the membrane. After 209 ps (see Figure 2), the number of helium atoms in both the gas and vacuum regions becomes equal and the system seems to reach an equilibrium state.

Figure 3 shows the number of permeated molecules as a function of simulation time together with the expected values from Knudsen flow, which are estimated from Eq. 6. The number of permeated molecules increases with time exponentially. This figure means that the steady state of flow is reached very quickly. This is rather consistent, considering the very thin membrane of the system and high mobility of He at 500 K. The MD values are very close to the Knudsen curve. Therefore, in agreement with previous experiments (Li and Hwang, 1992), the helium transport mechanism is a Knudsen flow. This result is consistent since the atomic size is small enough to allow He to enter the membrane pore, and the He–membrane interaction is not significant enough to form the adsorption phase, which are requirements for Knudsen flow.

CO_2 permeation

Figure 4 shows the permeation of CO_2 through the membrane at 500 K. The molecules diffuse and permeate as the simulation time increases. The number of CO_2 molecules in the vacuum region is considerably smaller than the number of He molecules. Figure 5 presents the number of permeated molecules as a function of time together with the Knudsen curve. At the beginning, the number of permeated molecules increases moderately; however, after 50 ps it rapidly increases beyond the estimated value from Knudsen flow. This result means that the flux of CO_2 needed 50 ps to come in a steady state of flow. This behavior is obviously different from that for He and implies that the transport of CO_2 is different from that of He.

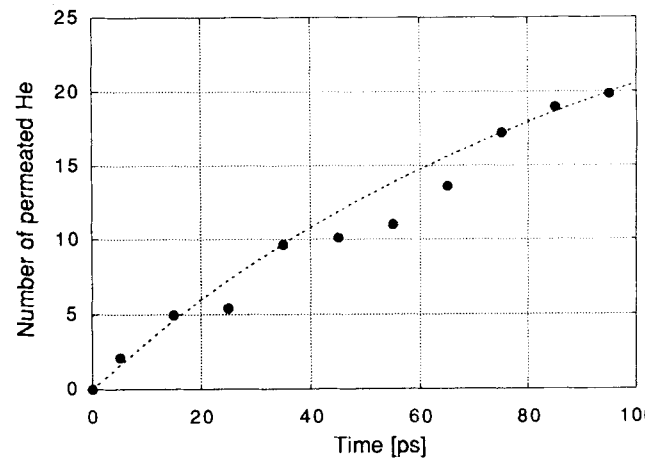

Figure 3. Time evolution of the number of permeated He atoms: MD results (dots) and Knudsen curve (dashed line).

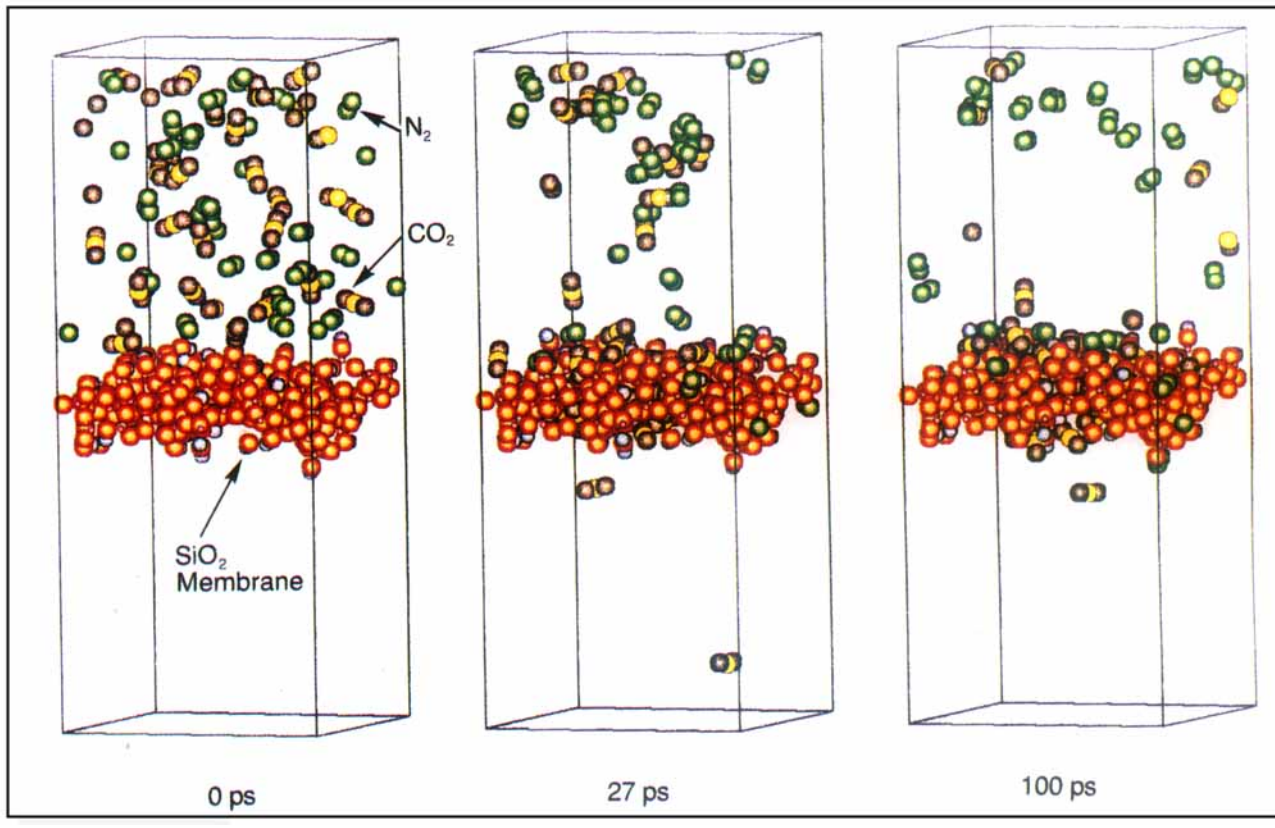

Figure 4. Permeation of the CO_2 single gas at 500 K.

Figure 6 shows the density profiles of CO_2 and He along the flow direction. In the case of He (Figure 6a), no strong peak near the membrane surface is observed, which means that He does not adsorb on the surface. Moreover, the density profile of He shows a distinct minimum at the center of the membrane in the direction of flow. This is because the pore structure is not cylindrical but narrow at the center of the pore, and the pore width at the inlet and outlet becomes broader. This may imply the rugged structure of the pore mouth. The broader spaces at the outlet and inlet of the pore allow for many molecules to stay there. In the case of CO_2, two strong peaks above and below the surface appear that are higher than the gas region or vacuum region peaks. This means that the density of CO_2 at both surfaces is higher than each region's individual density and that CO_2 adsorbs on the surfaces. Experiments have shown that the permeation of CO_2 through the silica membrane is strongly affected by its adsorption (Uhlhorn et al., 1992). From the real-time visualization, we observed that 96% of permeated helium atoms diffuse through the pore without adsorption. In contrast, 67% of permeated CO_2 molecules diffuse along the membrane surface. A higher peak at the surface of the vacuum region is partially due to the CO_2 molecules diffusing along the pore wall to the surface.

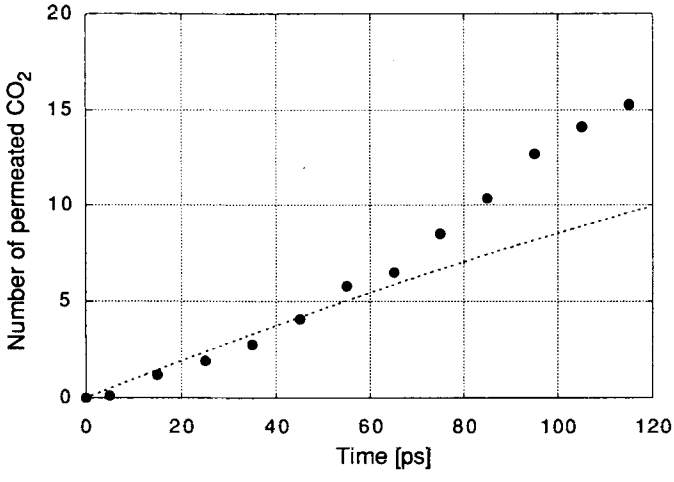

Figure 5. Time evolution of the number of permeated CO_2 molecules: MD results (dots) and Knudsen curve (dashed line).

N_2 permeation

We have performed MD simulation of N_2 permeation at 500 K. Figure 7 shows the time evolution of the number of permeated N_2 molecules. The permeance is lower than that estimated from Knudsen flow. Since no N_2 molecules permeate during the beginning 25 ps, the first 25 ps can be considered as the time to reach steady state. However, the permeance is still lower than that estimated from Knudsen flow if this period is considered, which means that another transport governs the N_2 permeation. Figure 8 shows the density profiles for N_2 along the flow direction. The presence of a strong

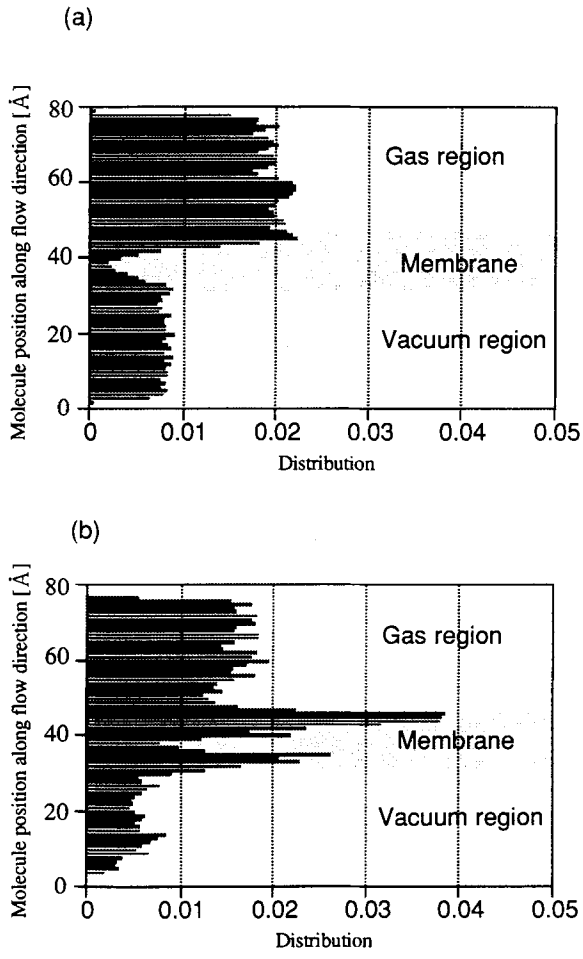

Figure 6. Density profiles along the flow direction for (a) He and (b) CO_2.

This was taken from MD result of single gas at 500 K between 10 ps and 30 ps.

peak over the membrane surface implies that N_2 molecules are also adsorbed like CO_2 molecules and even appear in the subsurface region within the silica network. However, unlike CO_2 this interaction does not promote the diffusion. The

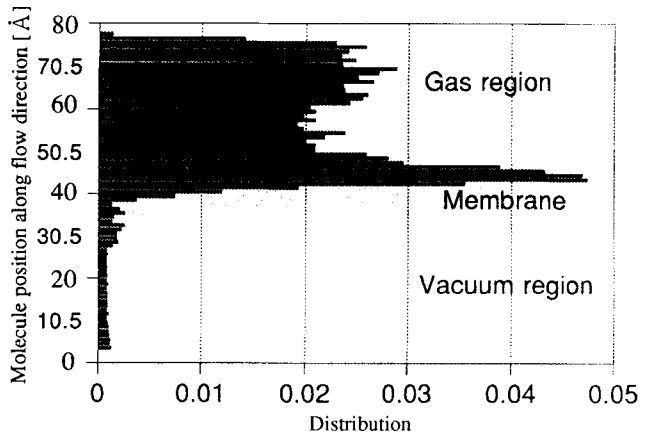

Figure 8. Density profiles along the flow direction for N_2.

This was taken from MD result of single gas at 500 K between 10 ps and 30 ps.

number of permeated N_2 molecules is smaller than that of CO_2, which is an unexpected result from Knudsen theory. In Figure 8 only one high peak appears, which is in contrast to the two peaks that appear in the case of CO_2. This is because, since the number of permeated N_2 molecules is very small, the peak at the surface in the vacuum region becomes small in relation to the peak at the surface in the gas region.

Figure 9 shows atomic trajectories for CO_2 and N_2 at an early stage of diffusion. The trajectories of CO_2 show that the molecules passed through all the space available inside the pore, whereas, within the same simulation time, very few N_2 molecules successfully passed. From real-time visualization we have seen that there were many attempts by N_2 molecules to permeate, but they often collided with the pore wall and returned to the gas region. From this figure the narrow channel of the pore structure at the center of the pore can be seen. Figure 10 gives the distribution inside the pore of the angle between the molecular axis (N–N or O–C–O) and the flow direction. This distribution shows the orientation of the molecules inside the pore. The free molecules in

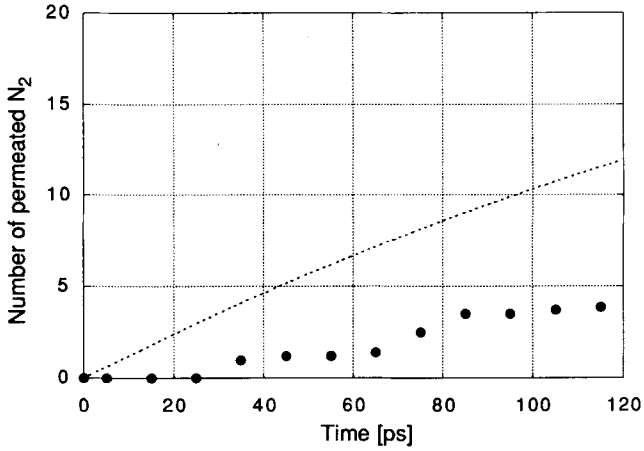

Figure 7. Time evolution of the number of permeated N_2 molecules: MD results (dots) and Knudsen curve (dashed line).

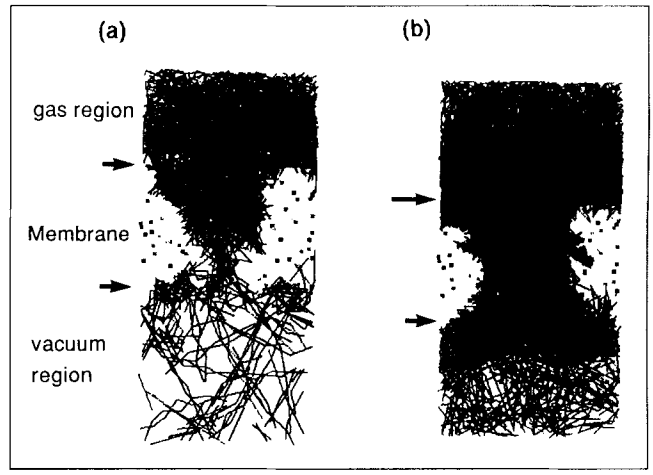

Figure 9. Trajectories of molecules that are permeating at 500 K: (a) N_2; (b) CO_2.

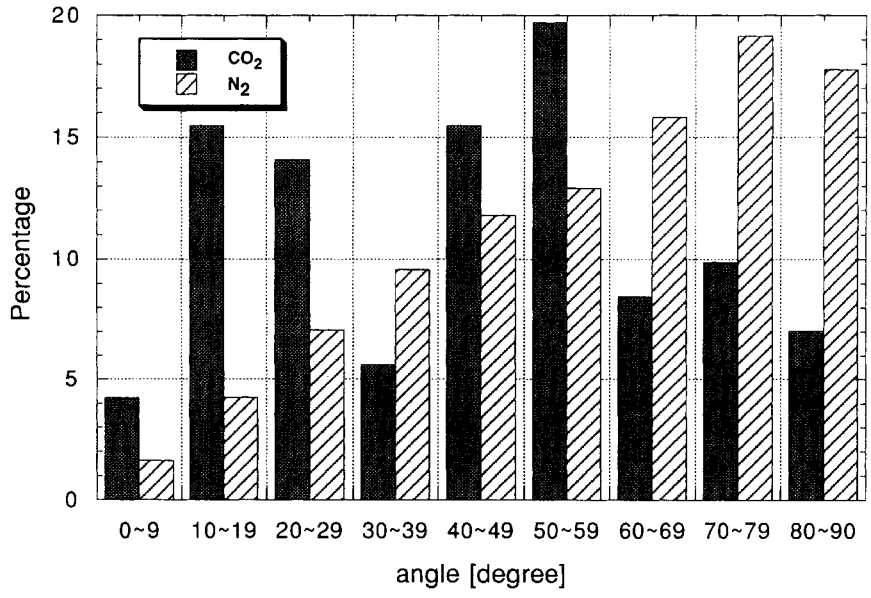

Figure 10. Distribution inside the pore of the angle between the molecular axis and the *z*-axis (flow direction).

the gas region are randomly oriented and present in all orientations. However, the interaction with the pore wall induces orientations that are suitable for adsorption. Most CO_2 molecules make an angle smaller than 60° with the flow direction, and are parallel to the pore wall. This orientation seems to be suitable for diffusion. However, most N_2 molecules make an angle larger than 60°. Therefore N_2 tends to be perpendicular to the pore wall, an orientation that does not promote diffusion. Although the length of O–C–O is larger than that of N–N, inside the pore the orientation of CO_2 relative to the pore wall makes its molecular size smaller than that of N_2. It seems that N_2's perpendicular orientation to the pore wall increases its apparent size and decreases the permeation rate.

Permeability analysis

The ratio of a single gas permeability to that of helium–single gas, which we call relative permeability, is given in Table 2. MD relative permeabilities are calculated from the number of permeated molecules after 100 ps from the first 60 ps. The first 60 ps, which is how long it takes to reach the steady state, were discounted. Both experimental and MD results are presented. Experimental values are in a wide range, and are sensitive to the structural aspects of the membrane (structure, pore size, and distribution). However, the experimental order of permeances is reproduced in MD simulations, and we find a decrease in the permeabilities in the order He > CO_2 > N_2.

Table 2. Relative Permeabilities to He: MD Calculation Results and Experimental Values

Membrane Structure	Author	Layer Thickness (nm)	Relative Permeability CO_2	Relative Permeability N_2
Silica-modified glass membrane	Okubo and Inoue (1989)	500	0.16 (523 K)	—
Silica-modified glass alumina	Uhlhorn et al. (1992)	60	0.46 (373 K)	—
Silicon-based glass membrane	Li and Hwang (1992)		0.58 (500 K)	0.22 (500 K)
Silica membrane	This study	1.4	0.78 (500 K)	0.22 (500 K)

Permeation of a mixed CO_2/N_2 gas

We have performed MD simulation of a mixed CO_2/N_2 gas permeation at 500 K. From the results of single-gas permeations, the larger permeance of CO_2 compared with N_2 is expected. Figure 11 shows MD results for the permeation of a mixed CO_2/N_2 gas. Initially 30 molecules of each species are present in the gas region. Both N_2 and CO_2 are adsorbed on the membrane surface. After 100 ps of simulation, only CO_2 diffusion was observed, and the permeated molecules are adsorbed at the bottom of the membrane surface. Therefore the membrane is selective and can separate CO_2 from a CO_2/N_2 mixture. In the vacuum region the ratio CO_2/N_2 in terms of the number of permeated molecules is larger than 5.

Figure 12 shows the time evolution of the number of permeated molecules. While the number of permeated CO_2 molecules increases with time, only one N_2 molecule succeeded in diffusing. From the real-time visualization, we observed that the permeated CO_2 molecules blocked the penetration of N_2 into the pore. Thus N_2 permeation is suppressed by that of CO_2. Furthermore, when comparing the permeation of the mixed gas with that of single gases (see Figures 5 and 7), we conclude that the permeation of each species decreases in the mixed gas. Therefore, in the mixed gas, species mutually alter their diffusions.

Conclusion

We used the MD method to investigate the dynamics of the permeation of He, N_2, and CO_2 molecules through a sil-

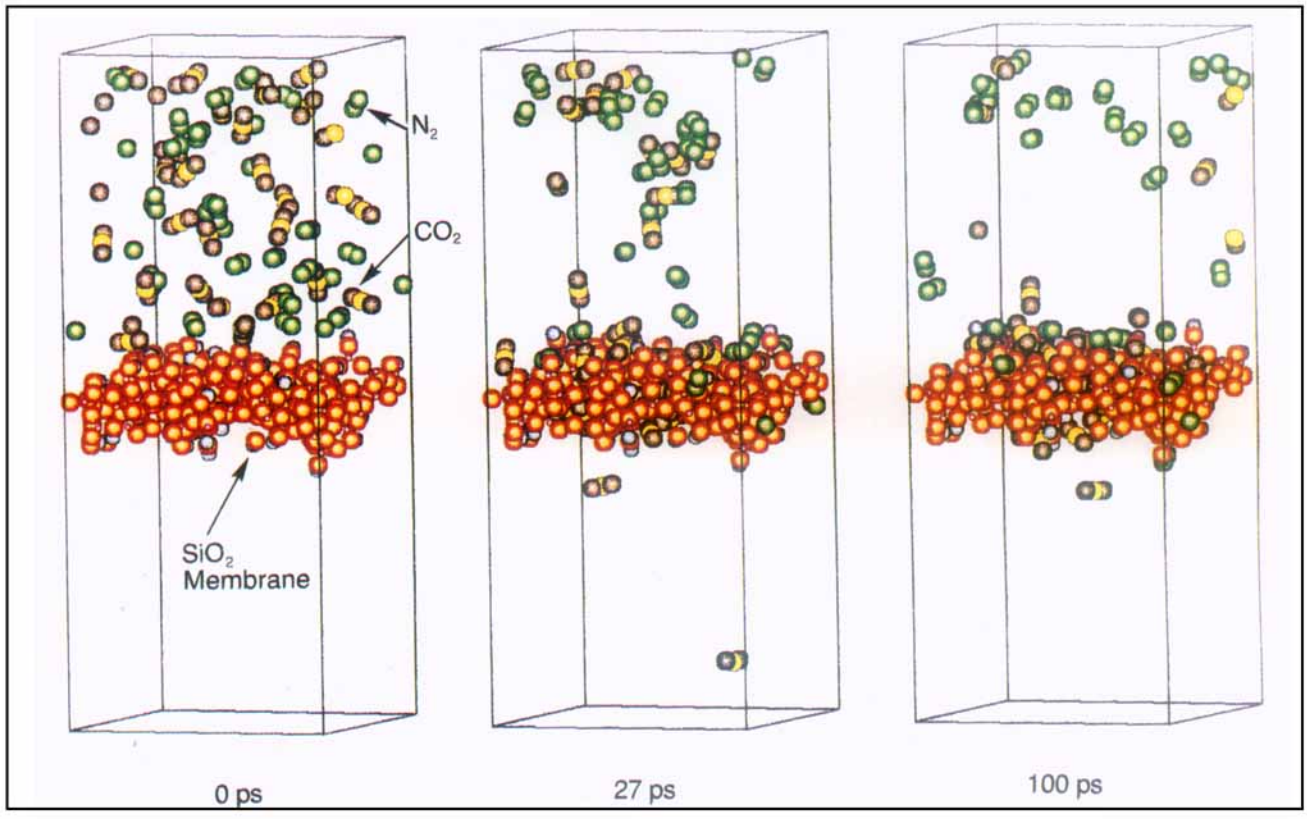

Figure 11. Permeation of the mixed CO_2/N_2 gas at 500 K; only CO_2 permeates.

ica-membrane model. Helium permeance is in good agreement with the value estimated from Knudsen flow. In contrast, CO_2 is adsorbed on the membrane surface and shows higher permeance than that of Knudsen flow. Inside the pore, CO_2 molecules tend to be parallel to the pore wall. This orientation appears to be suitable for diffusion. N_2 also interacts with the membrane surface. However, inside the pore, N_2 molecules tend to assume a perpendicular orientation to the pore wall, which decreases its diffusion. Although O–C–O length is longer than N–N distance, inside the pore the apparent size of N_2 is larger than that of CO_2. For a mixed CO_2/N_2 gas, selective CO_2 permeation was observed. Therefore, it is possible to separate CO_2 from the mixed gas.

While these results may overshadow the validity of the force field used, this work has demonstrated a reasonable consistency between MD permeabilities and Li and Hwang's experimental observation (1992). A detailed understanding of the entire permeation mechanism requires more sophisticated modes and methods, such as a grand canonical ensemble MD simulation technique. We are trying to achieve such a model, and hope to report on it in the near future.

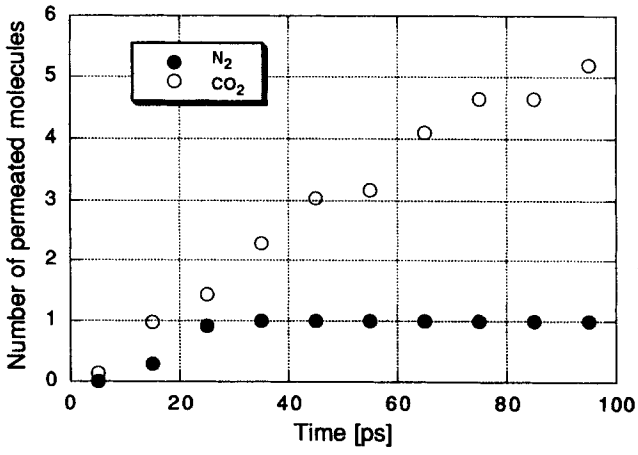

Figure 12. Time evaluation of the number of permeated CO_2 molecules (open circle) and N_2 molecules (closed circle).

Literature Cited

Bakker, W. J. W., F. Kapteijn, J. Poppe, and J. A. Moulijn, "Permeation Characteristics of a Metal-Supported Silicalite-1 Zeolite Membrane," *J. Memb. Sci.*, **117**, 57 (1996).

Carman, P. C., *Butterworths Scientific Publications*, Butterworths, London (1956).

Cheung, P. S. Y., and J. G. Powles, "The Properties of Liquid Nitrogen IV. A Computer Simulation," *Mol. Phys.*, **30**, 921 (1975).

Cracknell, R. F., D. Nichoson, and N. Quirke, "Direct Molecular Dynamics Simulation of Flow Down a Chemical Potential Gradient in a Slit-Shaped Micropore," *Phys. Rev. Lett.*, **74**, 2463 (1995).

Dauber-Osguthorpe, P., V. A. Roberts, D. J. Osguthorpe, J. Wolff, M. Genest, and A. T. Hagler, "Structure and Energetics of Ligand Binding to Proteins: Escherichia coli Dihydrofolate Reductase-Trimethoprim, A Drug-Receptor System," *Proteins: Struct., Funct., Genet.*, **4**, 31 (1988); *Discover User Guide*, Part I., Biosyn Technologies, CA (1933).

Fain, D. E., and G. E. Roettger, "Coal Gas Cleaning and Purification with Inorganic Membrane," *J. Eng. Gas Turbines Power*, **115**, 628 (1993).

Feuston, B. P., and S. H. Garofalini, 'Topological and Bonding Defects in Vitreous Silica Surfaces," *J. Chem. Phys.*, **91**, 564 (1989).
Furukawa, S., and T. Nitta, "Computer Simulation Studies on Gas Permeation through Nanoporous Carbon Membranes by Non-Equilibrium Molecular Dynamics," *J. Chem. Eng. Jpn.*, **29**, 725 (1996).
Gavalas, G. R., C. E. Megiris, and S. W. Nam, "Deposition of H_2-Permselective SiO_2 Films," *Chem. Eng. Sci.*, **44**, 1829 (1989).
Hagler, A. T., S. Lifson, and P. Dauber, "Consistent Force Field Studies of Intermolecular Forces in Hydrogen-Bonded Crystals. 2. A Benchmark for the Objective Comparison of Alternative Force Fields," *J. Amer. Chem. Soc.*, **101**, 5122 (1979).
Herzberg, G., *Spectra of Diatomic Molecules*, Van Nostrand Reinholt, New York (1950).
Hiby, J. W., and M. Pahl, *Z. Naturforsch*, **7a**, 542 (1952).
Hsieh, H. P., *Inorganic Membranes for Separation and Reaction*, Elsevier, Amsterdam (1996).
Hwang, S.-T., and K. Kammermeyer, *Techniques in Chemistry: Membranes in Separation*, Wiley-Interscience, New York (1975).
Iler, R. K., *The Chemistry of Silica*, Wiley, New York (1979).
Jiang, S., Y. Yan, and G. R. Gavalas, "Temporary Carbon Barriers in the Preparation of H_2-Permselective Silica Membranes," *J. Memb. Sci.*, **103**, 211 (1995).
Kawamura, K., *Molecular Dynamics Simulations*, F. Yonezawa, ed., Springer-Verlag, Berlin, p. 88 (1992).
Koros, W. J., and G. K. Fleming, "Membrane-Based Gas Separation," *J. Memb. Sci.*, **83**, 1 (1993).
Li, D., and S.-T. Hwang, "Gas Separation by Silicon Based Inorganic Membrane at High Temperature," *J. Memb. Sci.*, **66**, 119 (1992).
Misawa, M., D. L. Price, and K. Suzuki, "The Short-Range Structure of Alkali Disilicate Glasses by Pulsed Neutron Total Scattering," *J. Non-Cryst. Solids*, **37**, 85 (1980).
Miura, R., H. Yamano, R. Yamauchi, M. Katagiri, M. Kubo, R. Vetrivel, and A. Miyamoto, "Development of RYUGA for Three-Dimensional Dynamic Visualization of Molecular Dynamics Results," *Catal. Today*, **23**, 409 (1995).
Mizukami, K., H. Takaba, N. Ito, M. Kubo, A. Fahmi, and A. Miyamoto, "Permeability of Ar and He Through an Inorganic Membrane: A Molecular Dynamics Study," *Appl. Surf. Sci.*, **119**, 330 (1997).
Murthy, C. S., K. Singer, and I. R. McDonald, "Interaction Site Models for Carbon Dioxide," *Mol. Phys.*, **44**, 135 (1981).
Narten, A. H., "Diffraction Pattern and Structure of Noncrystalline BeF_2 and SiO_2 at 25°C," *J. Chem. Phys.*, **56**, 1905 (1972).
Okubo, T., and H. Inoue, "Single Gas Permeabilities Through Porous Glass Modified with Tetra Epoxy Silane," *AIChE J.*, **35**, 845 (1989).
Okubo, T., and T. Inoue, "Introduction of Specific Gas Selectivity to Porous Glass Membranes by Treatment with Tetraethoxylene," *J. Memb. Sci.*, **42**, 109 (1989).
Reid, R. C., J. M. Prausnitz, and B. E. Poling, *The Properties of Gases and Liquids*, 4th ed., McGraw-Hill, New York, p. 734 (1987).
Saracco, G., and V. Specchia, "Catalytic Inorganic Membrane Reactions: Present Experience and Future Opportunities," *Catal. Rev.-Sci. Eng.*, **35**, 305 (1994).
Sea, B.-K., K. Kusakabe, and S. Morooka, *J. Memb. Sci.*, **30**, 41 (1997).
Shelekhin, A. B., A. G. Dixon, and Y. H. Ma, "Theory of Gas Diffusion and Permeation in Inorganic Molecular-Sieve Membranes," *AIChE J.*, **41**, 58 (1995).
Sinclair, R. N., and A. C. Wright, "Static Approximation Distributions and Neutron Time-of-Flight Diffraction using the Harwell Linac," *Nucl. Instrum. Methods*, **114**, 451 (1974).
Takaba, H., K. Mizukami, M. Kubo, A. Stirling, and A. Miyamoto, "The Effect of Gas Molecule Affinities on CO_2 Separation from the CO_2/N_2 Gas Mixture Using Inorganic Membranes as Investigated by Molecular Dynamics Simulation," *J. Memb. Sci.*, **121**, 251 (1996).
Takaba, H., R. Koshita, K. Mizukami, Y. Oumi, N. Ito, M. Kubo, A. Fahmi, and A. Miyamoto, "Molecular Dynamics Simulation of Iso- and *n*-Butane Permeations Through a ZSM-5 Type Silicalite Membrane," *J. Memb. Sci.*, **134**, 127 (1997).
Tsuneyuki, S., M. Tukada, H. Aoki, and Y. Matsui, "First-Principles Interatomic Potential of Silica Applied to Molecular Dynamics," *Phys. Rev. Lett.*, **61**, 869 (1988).
Uhlhorn, R. J. R., K. Keizer, and A. J. Burggraaf, "Gas Transport and Separation with Ceramic Membranes: II. Synthesis and Separation Properties of Microporous Membranes," *J. Memb. Sci.*, **66**, 271 (1992).

Manuscript received June 23, 1997, and revision received Mar. 9, 1998.